Flexural Design Procedures for UHPC Beams and Slabs

Author(s) & Affiliation: Yiming Yao, Xinmeng Wang, Barzin Mobasher

School of Sustainable Engineering and the Built Environment, Arizona State University, Tempe, Arizona

Abstract:

Analytical solutions are developed for deflection calculations of determinate beams subjected to usual loading patterns. The solutions are based on a bilinear moment curvature response characterized by the flexural crack initiation and ultimate capacity based on a deflection hardening behavior. Equations for deflection distribution along the full length of a beam are presented for multiple cases including three- and four-point bending, which can be further extended to uniform load, concentrated moment, and cantilever beams. The proposed equations are capable of tracking the curvature, angle of rotation and deflection at any point along the beam as serviceability based design approach. A parametric study is conducted to examine the effects of moment and curvature at the ultimate stage to moment and curvature at the first crack ratios on the deflection. Results are examined for UHPC beams with different reinforcement types and test configurations. The accuracy of the present model is successfully verified.

Keywords: analytical, deflection, bilinear, moment-curvature, full range.

1. Introduction

Ultra-high performance concretes (UHPC) have been developed for their exceptional strength and durability properties. UHPC has attracted the growing interest of researchers in academia, engineers in the public and private sectors, and contractors across the world due to its highly enhanced mechanical and durability properties in comparison to conventional concrete. Exceptional mechanical properties of compressive strengths in excess of 22 ksi (150 MPa) and tensile strength of about 1-1.5 ksi (7-10 MPa) can be obtained (Wille et al. 2014). Design guidelines for UHPC are desired to address critical infrastructure criteria of sustainability, resiliency, and life-cycle design. This will be based on proper material parameter definitions, as well as a robust procedure to relate structure, properties, and behavior under loads. Most importantly, these procedures must also include critical key parameters for ductility, serviceability and sustainability.

Analytical and empirical expressions for moment vs. curvature or rotation relationships have been extensively used in modeling of load-deflection behavior, ultimate load capacity, as well as ductility of structures (Hillerborg 1990; Lopes and Carmo 2006). Extensive experimental and modelling approaches are availab1e for various structural members including beam and columns (Kheyroddin and Naderpour 2007; Sheikh and Yeh 1992), composite plates and slabs (Crisinel and Marimon 2004), steel girder bridges (Barth et al. 2004). Strain compatibility analysis has been used to obtain closed-form moment–curvature relationship for FRC and HRC beams, such as Taheri et al. (2011) as well as Van Zijl and Mbewe (2013). Solutions based on numerical methods were used to predict the load-middle span deflection response. Despite a widespread applicability, these procedures are impractical for general users since it requires numerical

methods programming and only simulates specific values such as the mid-span deflection. A more generalized and fast approach is desired for design procedure.

In this work analytical solutions of moment-curvature response of reinforced concrete section for strain hardening UHPC, hybrid reinforced concrete (HRC) are developed based on a parametrized bilinear moment-curvature. The advantage of using a bi-linear moment-curvature response is that material input parameters can be dramatically reduced which is beneficial for the development of design tools. The analytical moment-curvature is then used to obtain load vs. deflection response of a beam under typical statically determinate loadings. Furthermore, results of experimental tests conducted on a range of common structural sections are simulated to verify model applicability to a range of analytical moment-curvature responses for different materials used as input.

2. Model Derivation

2.1. Closed-form Moment-curvature Relationship

A general strain hardening tensile, and an elastic perfectly plastic compression model as derived by Soranakom and Mobasher (2008) and shown in Figure 1. Tensile response is defined by tensile stiffness, E, first crack tensile strain, ε_{cr}, Cracking tensile strength, $\sigma_{cr} = E\varepsilon_{cr}$, ultimate tensile capacity, $\alpha\varepsilon_{cr}$, and post crack modulus, $E_{cr}=\eta E$. The softening range is shown as a constant stress level, $\mu E\varepsilon_{cr}$. The compression response is defined by the compressive strength, σ_{cy} defined as $\omega\gamma E\varepsilon_{cr}$. The moment-curvature relationship is generated based on the tension and compression models discussed.

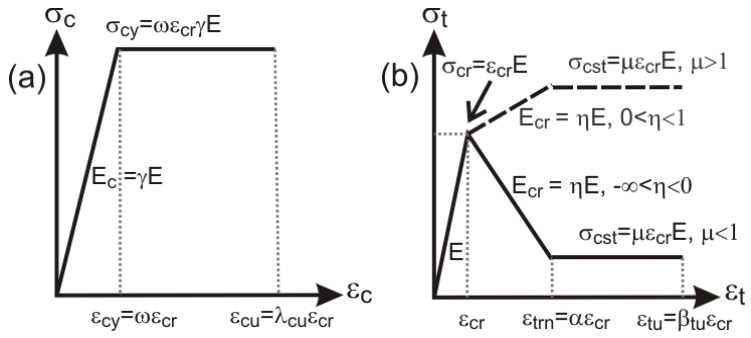

Figure 1. Material models for homogenized UHPC: (a) compression model and (b) tension model

Moment capacity of a beam section according to the imposed tensile strain at the bottom fiber ($\varepsilon_t = \beta\varepsilon_{cr}$) can be derived based on the assumed linear strain distribution as shown in Figure 2. For example, Figure 2 shows the strain and stress distributions of cross-section in different stages as defined by Soranakom and Mobasher (2008). The corresponding strain and stress distributions of other stage also can be generated by flowing the tension and compression models. Force components and their distance to the neutral axis can be expressed as:

$$\frac{F_{c1}}{bd\sigma_{cr}} = \frac{\beta\gamma k^2}{2(1-k)}; \qquad \frac{y_{c1}}{d} = \frac{2}{3}k \tag{1}$$

$$\frac{F_{t1}}{bd\sigma_{cr}} = \frac{(1-k)}{2\beta} \quad ; \qquad \frac{y_{t1}}{d} = \frac{2}{3}\frac{(1-k)}{\beta} \tag{2}$$

$$\frac{F_{t2}}{bd\sigma_{cr}} = \frac{(1-k)(\beta-1)(\eta\beta-\eta+2)}{2\beta} \quad ; \qquad \frac{y_{t2}}{d} = \frac{2\eta\beta^2-\eta\beta-\eta+3\beta+3}{3\beta(\eta\beta-\eta+2)}(1-k) \tag{3}$$

where F and y are the force and its centroid, respectively; subscripts *c1,t1,t2* designate compression zone 1, tension zone 1 and 2, respectively; b and d are the width and the height of the beam, respectively. The neutral axis parameter k is found by solving the equilibrium of net internal forces equal to zero, $F_{c1} + F_{t1} + F_{t2} = 0$.

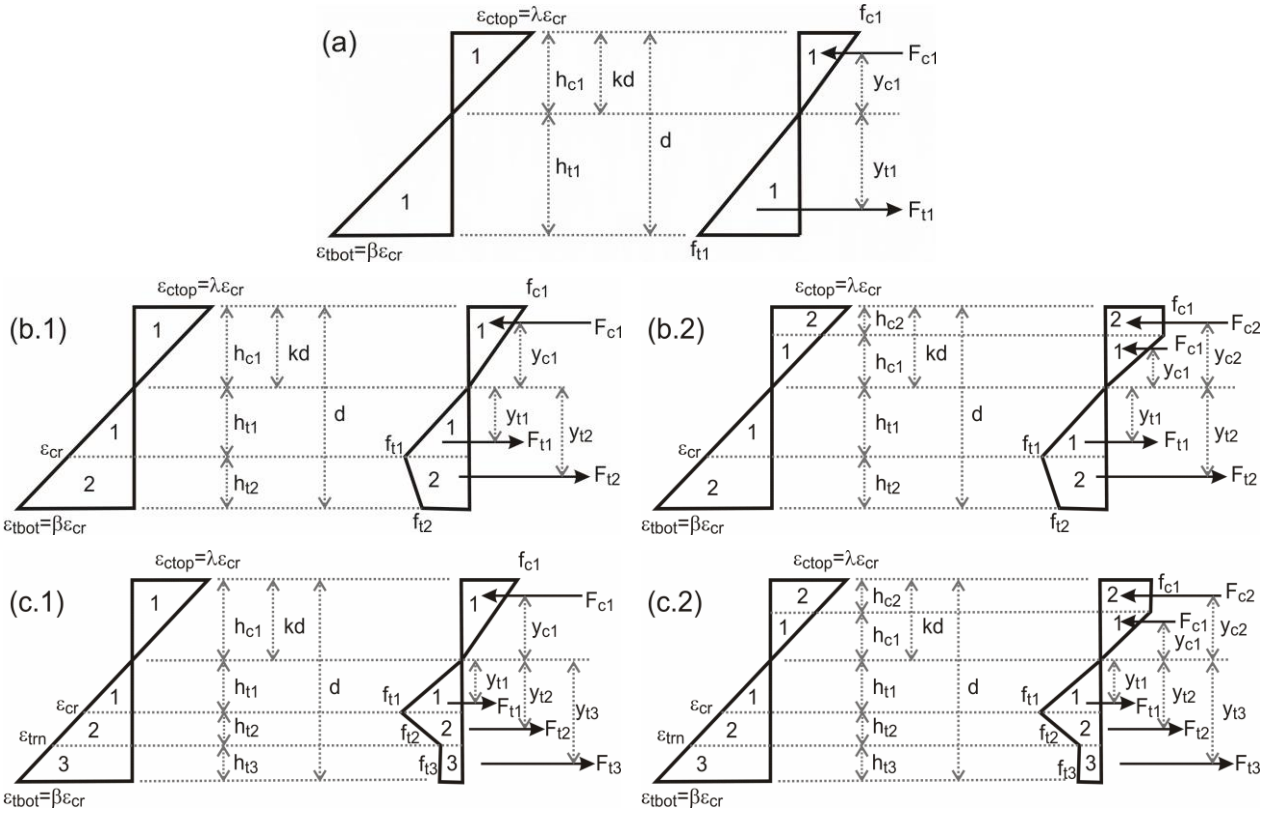

Figure 2. Stress–strain diagram at different stages of normalized tensile strain at the bottom fiber (β): (a) $0 \le \beta \le 1$ and $\lambda \le \omega$; (b.1) $1 < \beta \le \alpha$ and $\lambda \le \omega$; (b.2) $1 < \beta \le \alpha$ and $\omega < \lambda \le \lambda_{cu}$; (c.1) $\alpha < \beta \le \beta_{tu}$ and $\lambda \le \omega$; (c.2) $\alpha < \beta \le \beta_{tu}$ and $\omega < \lambda \le \lambda_{cu}$ (Soranakom and Mobasher 2008).

The neutral axis parameter k is found by solving the equilibrium of net internal forces and the nominal moment capacity M_n is obtained by taking the first moment of force about the neutral axis. Closed-form equations of moment and curvature at different stages for FRC and HRC sections can be found in (Soranakom and Mobasher 2008; Mobasher et al. 2015). Figure 3 shows an example of the normalized moment-curvature and linearized portions for deflection-hardening material which can be exhibited by UHPC. Similarly, one can use commercially available or open sources programs to generate the moment-curvature responses for given cross section, and subsequently linearize them.

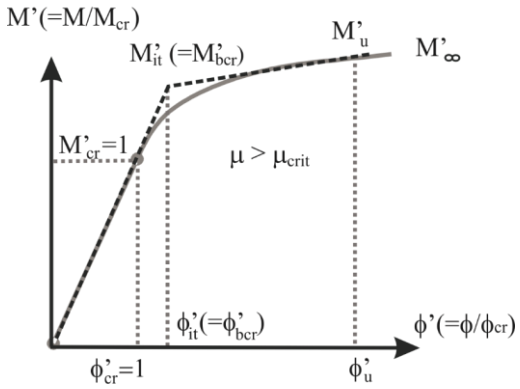

Figure 3. Normalized moment-curvature diagram and approximate bilinear model for deflection hardening ($\mu > \mu_{crit}$).

2.2 Bilinear moment-curvature relationship

Figure 4 presents the simplified parametric moment-curvature response as a bilinear function including elastic stage (Stage 1) and post-crack stage (Stage 2). As shown in Figure 4a, the elastic range of moment increase with a slope of EI_g up to the first flexural cracking moment of coordinates (φ_{cr}, M_{cr}), where $M_{cr} = bd^2 E\varepsilon_{cr} / 6, \varphi_{cr} = 2\varepsilon_{cr} / d$. The post-crack region is characterized by a reduced stiffness EI_{cr} and extends to the ultimate flexural capacity (φ_u, M_u) which corresponds to the limit state of plastic hinge formation, or associated with a specified maximum curvature, maximum tensile or compressive strain, depending on the specified limit state or flexural failure criteria. The bilinear moment-curvature response is defined by two control points (M_{cr}, φ_{cr}) and (M_u, φ_u) and expressed using linear functions as:

$$M(\varphi) = EI_g \phi \qquad 0 < M \le M_{cr} \qquad 0 < \varphi \le \varphi_{cr}$$

$$M(\varphi) = \frac{M_u - M_{cr}}{\varphi_u - \varphi_{cr}}(\varphi - \varphi_{cr}) + M_{cr} \qquad M_{cr} \le M \le M_u \qquad 1 \le \varphi \le \varphi_u \tag{4}$$

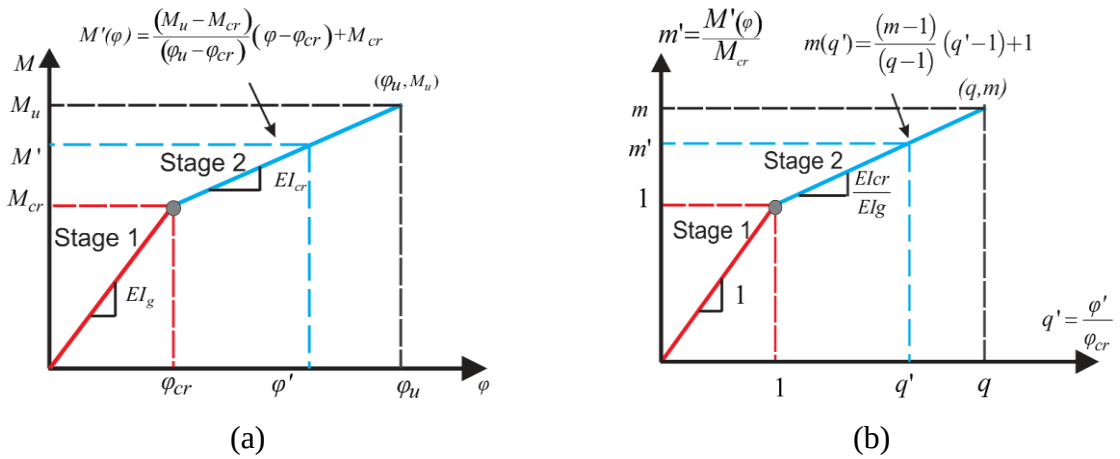

Figure 4. Parametric moment-curvature relationship: (a) bilinear representation; (b) dimensionless moment-curvature curve represented as variables (q', m').

Equations 4 can be normalized with respect to cracking moment M_{cr}, resulting in dimensionless moment m' and curvature q' as illustrated in Figure 4b.

2.3. Statically Determinate Systems

A case of three-point bending of a prismatic beam as shown in Figure 5 illustrates the moment and curvature distributions as well as the subsequent derivation of load-deflection solutions. Different stages of bilinear moment-curvature relationship (c.f. Figure 3) and regions along a beam (c.f. Figure 4), create several piecewise linear distributions.

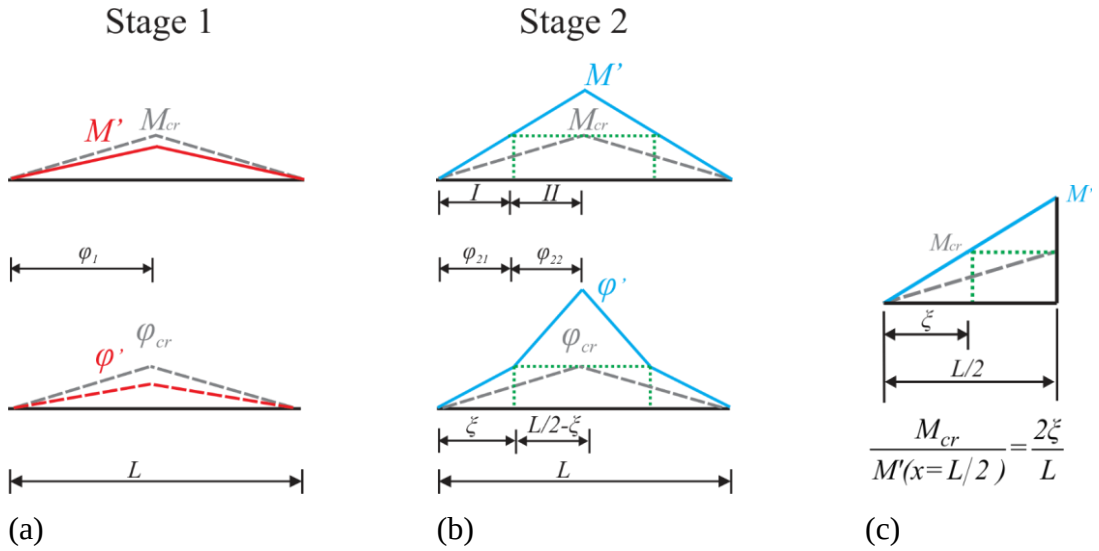

Figure 5. Moment and curvature distribution along the beam (a) prior to cracking, (b) after cracking, (c) calculation of ξ by means of similar triangles.

As shown in Figure 5a, during Stage 1 for the linear elastic beam prior to the first flexural crack ($0 \le M'(L/2) \le M_{cr}$), the curvature is linearly related to the bending moment diagram throughout the beam as shown in Figure 3. Similar triangles are used to express the bending moment and curvature as a function of the location x (only half of the beam is considered due to the symmetric condition):

$$M'(x)=\frac{2x}{L}M'(x=L/2)$$
$$\varphi_1(x)=\frac{2x}{L}\varphi'(x=L/2) \qquad 0<x<\frac{L}{2} \tag{6}$$

By taking double integration of the curvature throughout the length of beam, one can obtain the equations for mid-span deflection as follows:

$$\delta_1^* = \frac{\delta_1}{\varphi_{cr} L^2} = \left(\frac{x^3}{3L^3} - \frac{x}{4L}\right) q', \qquad 0<x<\frac{L}{2} \tag{7}$$

$$\delta_{2,I}^{*}=\frac{x^3}{6L^2\xi}-\frac{(L+Lq'-2q'\xi)x}{4L^2},\qquad 0\le x\le\xi$$

$$\delta_{2,II}^{*}=\frac{1}{L-2\xi}\left(\frac{(q'-1)x^3}{3L^2}+\frac{(L-2q'\xi)x^2}{2L^2}+\frac{x(4q'\xi-L-Lq')}{4L}+\frac{\xi^2(L-2q'\xi)}{6L^2}\right),\quad \xi\le x\le\frac{L}{2} \tag{8}$$

The subscripts of "1" and "2" refer to curvature in Stages 1 and 2. The symbol of asteroid indicates that the deflections normalized with respect to material properties and geometries. The actual deflection can be obtained by multiplying a factor of $\varphi_{cr}L^2\delta_1^*$, For example, $\delta_1=\varphi_{cr}L^2\delta_1^*$.

A similar approach has been applied to a variety of combinations of beam types including four-point bending, cantilever, over-hang and loading conditions with detail derivations and results presented by Wang (2015).

3. Parametric Study

Parametric study is conducted by using a set of material models to generate moment-curvature response. Two primary model variables *m* and *q* which can be obtained for various beam types and material properties are evaluated in a parametric study presented next. Figure 6 shows the profiles of deflection coefficients for a three-point bending beam when *m* and *q* range from 1.2-2.0 and 2-5, respectively, using equations (7) and (8). The sign convention is defined as downward negative.

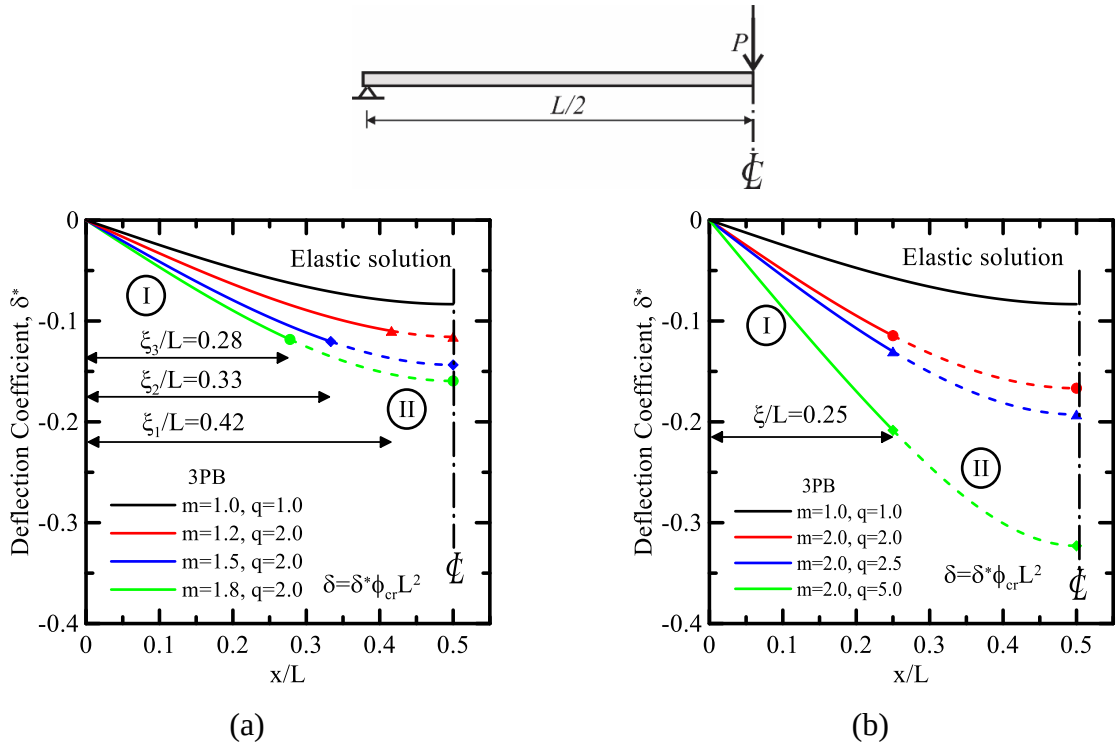

Figure 6. Effects of (a) normalized moment *m* and (b) normalized curvature *q* on the deflection distribution of a beam subjected to three-point bending.

Figure 6a shows the deflection coefficient at three levels of ultimate curvature (q_1, q_2, q_3) in a three-point bending beam. The model parameters m = 2 implies that the ultimate moment is twice of the cracking moment. Increase in the ultimate curvature q from 2 to 5 indicates a reduction in post-crack stiffness. As the post-crack stiffness decreases, the deflection increases for as much as 50%. Different regions of I (solid lines) and II (dashed lines) are also identified in the figures by the length of region I, defined as parameter ξ. If the maximum moment m is held constant in this exercise, ξ is also a constant and equal to 0.25 for m = 2 (as it is a function of L & m). As m increases, ξ decreases indicating that a larger portion of the beam is in the cracked region with higher load. As a comparison, the elastic solution at the end of Stage 1, i.e., m= q=1, is also plotted.

4. Experimental Verification of the Analytical Model

The applicability and accuracy of the proposed model are verified against the experimental data of various beams tested by different researchers. Yang et al. (2010) tested full scale UHPC beams with 2.7m span under four-point bending. The beam was reinforced by steel rebar of 0.9% with addition of 2% steel fiber. The comparison between experimental and simulated responses is shown in Figure 7a. The parameters used in the model include Young's modulus E = 51GPa, first crack tensile strain ε_{cr} = 300$\mu\varepsilon$, and stiffness ratio η = 0.25. Limit parameters for m and q were used as 3.4 and 10.5, respectively. Figure 7b compares the responses of a full scale beam reinforced with steel fiber only, tested by di Prisco et al. (2013). The beam span is 3.0m and the fiber volume fraction is 1.2%. As plain FRC beam, the levels of ultimate load and ductility are much lower compared to the beams with longitudinal reinforcements. Yoo and Yoon (2015) tested UHPC beams with a hybrid reinforcements including 0.94% of rebar and 2% of smooth steel fiber. The comparison is illustrated in Figure 7c where the model parameters are indicated. According to the parametric studies conducted by Mobasher et al. (2015), the normalized moment capacity dramatically increased from 6.3 to 13.1 as the reinforcement ratio increased from 0.01 to 0.03. The improvement due to addition of fibers was marginal compared to longitudinal rebars. The present modelling of hybrid section is an extension of the analytical study on moment-curvature responses.

In addition to traditional steel rebars, GFRP bars have also been used to reinforce UHPC beams with steel fibers studied by Yoo et al. (2016). Full scale beams with 0.5% of GFRP bars and 2% of steel fiber were tested under three-point bending. The cross section of the beam is 200mm by 270mm while the beams tested by Yang et al. has a section of 180mm by 270mm. It is also noted that the model parameters of the two sets of simulations are quite similar except the stiffness ratio and η ultimate curvature q. Compared to steel rebar, the beams reinforced by GFRP bars exhibit lower stiffness but higher ductility, which is attributed to the differences in the mechanical properties of steel and GFRP. It is also noted that the load-deflection responses exhibit a plateau stage while approaching the maximum ductility, which is due to the yielding of tensile steel. This has also been captured by the authors' previous analytical work (Mobasher et al. 2015). In present study, the steel yielding stage is simply represented by a constant moment value. The simulated results are quite favorable for different materials and test configurations.

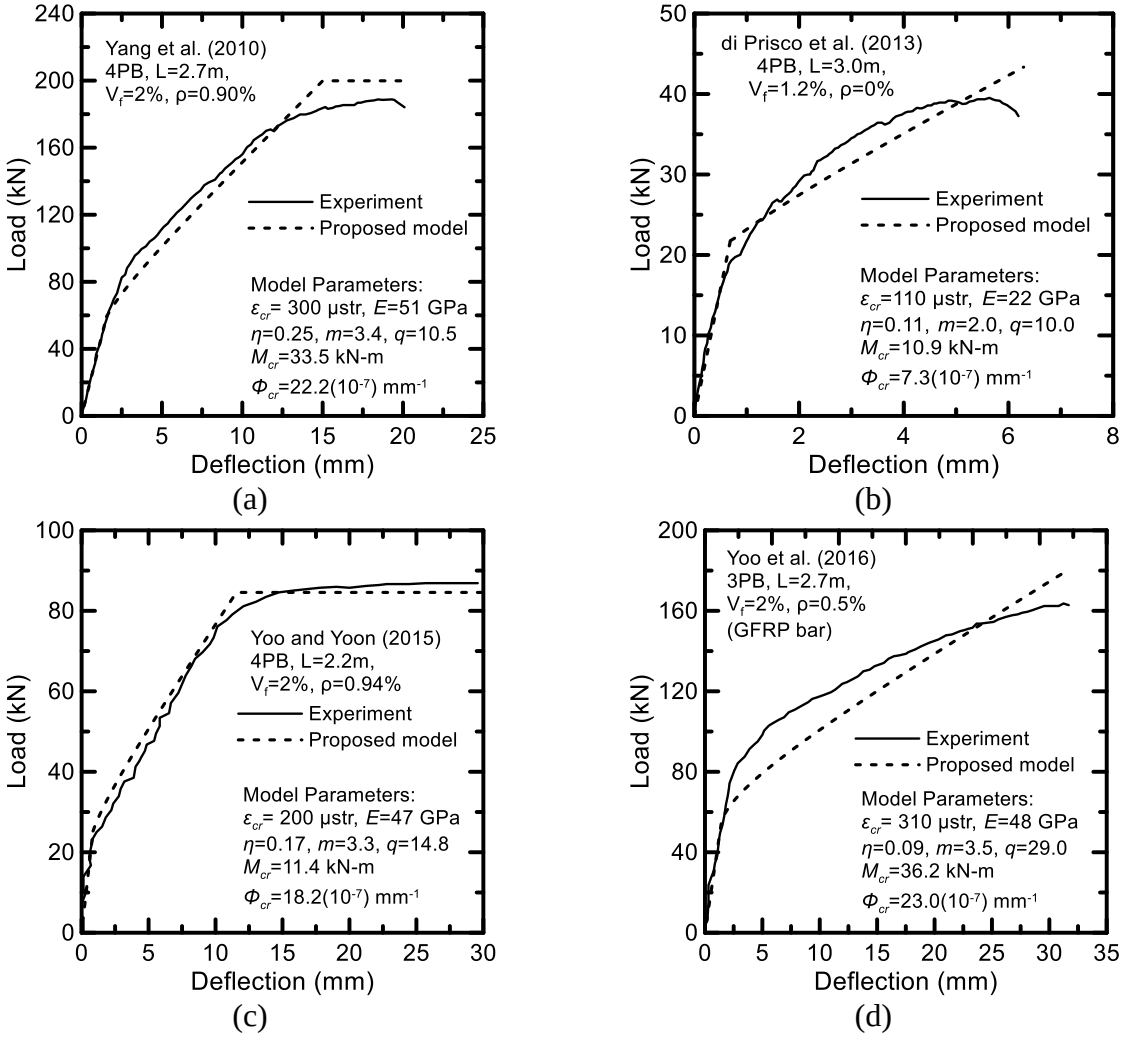

Figure 7. Comparison between experimental data and proposed model for the beams tested by (a) Yang et al. (2010), (b) di Prisco et al. (2013), (c) Yoo and Yoon (2015), (d) Yoo et al. (2016).

5. Conclusions

A bilinear moment-curvature relationship defined by the flexural crack initiation and ultimate capacity is proposed as basis for the derivation of an analytical load-deflection model exhibiting deflection hardening behavior. The analytical solutions characterize the full range distribution of curvature, angle of rotation, and deflection responses at any given point along the beam. Various types of beams and loading conditions are addressed such as three-point bending, four-point bending, uniform loads, concentrated moment on simple beams and cantilever beams.

A parametric study examines the effect of moment-curvature bilinear parameters on the load-deflection response. Simulations are conducted to predict the flexural responses of UHPC beams with different reinforcement types, cross sectional properties, geometries and testing configurations. The accuracy of the proposed model is successfully verified.

6. References

Barth, K.E., Hartnagel, B.A., White, D.W., and Barker, M.G. "Recommended procedures for simplified inelastic design of steel I-girder bridges." *Journal of Bridge Engineering,* Vol. 9, No. 3, May 2004, pp. 230-242.

Crisinel, M., and Marimon, F. "A new simplified method for the design of composite slabs." *Journal of Construction Steel Research,* Vol. 60, No. 3, March 2004, pp. 481-491.

di Prisco, M., Colombo, M., and Dozio, D. "Fibre-reinforced concrete in fib Model Code 2010: principles, models and test validation." *Structural Concrete,* V. 14, No. 4, 2013, pp. 342-361.

Hillerborg A. "Fracture mechanics concepts applied to moment capacity and rotational capacity of reinforced concrete beams" *Engineering Fracture Mechanics,* 1990; V. 35, No. 1, pp.233-240.

Kheyroddin, A., and Naderpour, H. "Plastic hinge rotation capacity of reinforced concrete beams." *International Journal of Civil Engineering (IJCE),* Vol., 5, No. 1, 2007, pp. 30-47.

Lopes, S.M., and do Carmo, R.N., "Deformable strut and tie model for the calculation of the plastic rotation capacity. *Computers&Structures,* Vol. 84, No. 31, Dec. 2006, pp. 2174-2183.

Mobasher, B., Yao, Y., Soranakom, C. Analytical solutions for flexural design of hybrid steel fiber reinforced concrete beams. *Engineering Structures,* Vol. 100, October 2015, pp. 164-177.

Sheikh, S., and Yeh, C. "Analytical Moment-Curvature Relations for Tied Concrete Columns." *Journal of Structural Engineering,* Vol. 118, No. 2, February 1992, pp. 529–544.

Soranakom, C., Mobasher, B. "Closed-Form Solutions for Flexural Response of Fiber-Reinforced Concrete Beams." *Journal of Engineering Mechanics,* Vol. 133, No. 8, August 2007, pp. 933-941.

Soranakom, C., Mobasher, B. "Correlation of tensile and flexural response of strain softening and strain hardening cement composites." *Cement and Concrete Composites,* Vol. 30, July 2008, pp. 465-477.

Taheri, M., Barros, J., and Salehian, H. "A design model for strain-softening and strain-hardening fiber reinforced elements reinforced longitudinally with steel and FRP bars." *Composites Part B: Engineering,* Vol. 42, No. 6, September 2011, pp. 1630–1640.

Wang, X. Analytical Load-Deflection Equations for Beam and 2-D Panel with a Bilinear Moment-Curvature Model. Thesis, 2015, Arizona State University. Tempe, Arizona.

Wille, K., El-Tawil, S., and Naaman, A. E. "Properties of strain hardening ultra high performance fiber reinforced concrete (UHP-FRC) under direct tensile loading." *Cement and Concrete Composites,* Vol. 48, April 2014, pp. 53-66.

Yang, I. H., Joh, C., and Kim, B. S. "Structural behavior of ultra high performance concrete beams subjected to bending." *Engineering Structures,* Vol. 32, No. 11, November 2010, pp. 3478-3487.

Yoo, D. Y., Banthia, N., and Yoon, Y. S. "Flexural behavior of ultra-high-performance fiber-reinforced concrete beams reinforced with GFRP and steel rebars." *Engineering Structures,* Vol. 111, March 2016, pp. 246-262.

Yoo, D. Y., and Yoon, Y. S. "Structural performance of ultra-high-performance concrete beams with different steel fibers." *Engineering Structures,* Vol. 102, November 2015, pp. 409-423.

Zijl, GPAG., and Mbewe, PBK. "Flexural modelling of steel fibre-reinforced concrete beams with and without steel bars." *Engineering Structures,* Vol. 53, August 2013, pp. 52–62.